Unravelling geological controls on groundwater flow and surface water-groundwater interaction in mountain systems: A multi-disciplinary approach

Etienne Marti, Sarah Leray, Daniela Villela, José Maringue, Gonzalo Yáñez, Esteban Salazar, Fernando Poblete, José Jimenez, Gabriela Reyes, Guillermo Poblete, et al.

Unravelling geological controls on groundwater flow and surface water-groundwater interaction in mountain systems: a multi-disciplinary approach

Authors: Etienne Marti[1,2], Sarah Leray[2,3,*], Daniela Villela[4], José Maringue[5], Gonzalo Yáñez[5], Esteban Salazar[4], Fernando Poblete[6], José Jimenez[2], Gabriela Reyes[6], Guillermo Poblete[2], Zeidy Huamán[2], Ronny Figueroa[5,Φ], Jaime Araya Vargas[5,¥], Jorge Sanhueza[5], Marjorie Muñoz[7], Reynaldo Charrier[6,7], Gabriel Fernández[2]

[1] Université de la Sorbonne, Paris, France

[2] Departamento de Ingeniería Hidráulica y Ambiental, Pontificia Universidad Católica de Chile, Santiago, Chile

[3] Centro de Cambio Global UC, Pontificia Universidad Católica de Chile, Santiago, Chile

[4] Servicio Nacional de Geología y Minería, Santiago, Chile

[5] Departamento de Ingeniería Estructural y Geotecnia, Pontificia Universidad Católica de Chile, Santiago, Chile

[6] Departamento de Geología, Facultad de Ciencias Físicas y Matemáticas, Universidad de Chile, Santiago, Chile

[7] Carrera de Geología, Universidad Andrés Bello, Santiago, Chile

[¥] Now at Departamento de Geología, Universidad de Atacama, Copiapó, Chile

[Φ] Now at Centro de Estudios Avanzados en Zonas Áridas (CEAZA), La Serena, Chile

[*]Corresponding author: saleray@ing.puc.cl

Av. Vicuña Mackenna 4686, Macul, Región Metropolitana, Chile

Abstract

Mountain water resources are considered to be the world's water towers. Still, despite their importance for downstream societies and ecosystems and their vulnerability to climate change, they remain poorly understood – It is the case in particular of mountain groundwater systems. Their complexity makes them difficult to conceptualize, while their remoteness makes them difficult to study, both observationally and instrumentally. Understanding mountain hydrogeological systems is mostly limited by the lack of characterization of the subsurface geologic framework and by the limited understanding of the role of geological structures on groundwater flow and on surface water-groundwater interaction. Removing methodological barriers is therefore a necessary step for improving the understanding of mountain hydrogeological systems.

To tackle this problem, we develop a comprehensive multi-disciplinary approach to gain insights into the hydrogeological role of geological structures in ungauged mountain catchments. The methodology consists of several complementary methods: (1) geological mapping at multiple scales; (2) a geophysical study including on-ground Electrical Resistivity Tomography (ERT) and, gravimetry transects, and a UAV-based magnetic survey; (3) hydraulic data, including a 9 km long transect of streamflow measurements in the recession period, the long-term Normalized Difference Vegetation Index (NDVI), and varied hydric markers (e.g., a thermal spring and a puddle). The methodology is tested in the Parque Nacional del Río Clarillo, an ungauged catchment in the Andes Mountains (≈ 130 km^2) that is illustrative of the complexity of mountain hydrosystems featuring fault zones, weathered zones, intrusive rocks, and volcano-sedimentary successions.

An increase of approximately 50% in the streamflow is observed over a short distance of 1 km. Such a localized and significant increase in the baseflow is not related to any superficial supply and can only be explained by groundwater exfiltration. Based on the multiscale geological mapping and geophysical

survey, a regional N-S fault and a secondary set of E-W local faults are identified in the vicinity of the resurgence area, which conjointly are likely to export groundwater from a neighbouring subcatchment up to the resurgence area. Downstream of the resurgence area, no significant change in the baseflow is observed, corresponding to the presence of an impermeable granitic pluton identified by the geological and geophysical mapping. Finally, a fractured zone in the Andean foothills is identified in the volcanic unit, which coincides with a perennial thermal spring, indicating upwelling flow and hydrogeological connectivity between the mountain block and the alluvial basin.

The results strongly support the ability of the proposed methodology to identify geological structures that substantially impact the evolution of the baseflow through the catchment. The complementary multi-disciplinary methods are used innovatively to infer the link between geological and hydrogeological structures. The methodology does not aim to fully characterize the geological framework of the catchment but pragmatically focuses on hydrogeologically pertinent structures that may impact baseflow and consequently catchment management.

Keywords: Structural geology, UAV-based magnetic, hydrogeophysics, fault zone, mountain aquifer, groundwater-surface water interaction

1. Introduction

Interest in mountain catchments has been growing recently (Markovich et al., 2019 and references within). Mountains serve as water reservoirs for downstream alluvial basins due to the heavy precipitation they receive (Immerzeel et al., 2020; Somers and McKenzie, 2020). More than half of humanity depends on mountain hydrosystems for their water supply (Grêt-Regamey et al., 2012). Snow- and glacier-dominated hydrosystems supply more than one-sixth of the world's population

(Barnett et al., 2005). Human dependence on these systems is all the more critical as they are particularly vulnerable to climate change (Beniston, 2003; Huss et al., 2017; Viviroli et al., 2011). Understanding the functioning of mountain blocks and their hydraulic connectivity with anthropized basins downstream is thus critical for water resource management (Kamenik et al., 2001; McDonnell, 2003; Soulsby et al., 2007), as well as for society's resilience to climate change (Hayashi, 2020; Viviroli et al., 2020). Furthermore, mountain catchments constitute preserved spaces and biosphere reserves, in some cases harbouring endemic or native species (Clarke et al., 2008; Freeman et al., 2007; Meyer et al., 2007) and providing various ecosystem services (Egan and Price, 2017).

However, despite their importance, mountain hydrogeological systems remain poorly understood (Bishop et al., 2008) owing to their inherent complexity stemming from significant topographic, climatic, and geological gradients. In particular, the interplay of geology, geomorphology, and climate on groundwater flow and related variables is barely understood (Condon and Maxwell, 2015; Gleeson and Manning, 2008; Winter, 2001): for example, groundwater-flow scale, depth, distribution (Markovich et al., 2019; Roques et al., 2014), and recharge (McCord et al., 1997; Nicolas et al., 2019; Sanford, 2002; White and Burbey, 2007), groundwater-surface water interaction (Brunner et al., 2009; Fleckenstein et al., 2010), groundwater timescales (Jasechko et al., 2016), and river ecology and biogeochemistry (Kolbe et al., 2016; Weyer et al., 2014). The geological heterogeneity of mountain blocks related to multiscale fracturing, lithological discontinuities, weathering, etc., is likely to substantially control groundwater flow as significant gradients of the hydraulic conductivity induce flow anisotropy (Leray et al., 2013, 2012), flow channelling, intercatchment flow (Fan, 2019), and possibly groundwater exfiltration (Bense et al., 2013; Caine et al., 1996; Scibek et al., 2016).

Although studies indicate that geological structures substantially impact groundwater-surface water interaction (Schaller and Fan, 2009) and stream flowrate and regime, most studies have focused on the role of climate and geomorphology (Condon and Maxwell, 2015; Cuthbert et al., 2019; Gleeson and Manning, 2008; Welch and Allen, 2012). The geological complexity of hydrogeological systems

strongly impedes the generalization of in situ observations and site-specific results and accordingly limits the development of unified hydrogeological frameworks (Markovich et al., 2019; Wilson and Guan, 2004). Worse, mountain hydrogeological systems remain mainly uncharacterized as their steep topographic gradients and remoteness strongly limit access and site instrumentation. The scientific bottleneck regarding the understanding of the hydrogeological functioning of mountain groundwater systems is therefore above all a methodological gap, the filling of which requires the improved characterization of their subsurface geologic framework (Bense et al., 2013; Markovich et al., 2019).

Groundwater flow paths and origins in mountain catchments have traditionally been inferred using hydrogeochemistry, water stable isotopes, and environmental tracers such as noble gases and anthropogenic tracers (Alvarez-Campos et al., 2022; Baraer et al., 2015; Hilberg, 2016; Jung et al., 2021; Ma et al., 2018; Manning and Solomon, 2005). As they directly derive from flow processes, these methods can theoretically compensate for the lack of direct observations of hydraulic conductivity and hydraulic gradients from standard hydraulic methods (boreholes, pumping tests) (Ginn et al., 2009). However, because of water mixing processes, they constitute integrative methods that remain poorly effective to differentiate between hydrogeological models at the local scale (Troldborg et al., 2007) and to identify hydrogeologically pertinent structures in complex systems (Leray et al., 2012). Hence, in the absence of end-member waters with significantly different chemical signatures, the deconvolution of tracers and hydrogeochemical data is extremely challenging.

Water balance analysis is a straightforward method that has been mainly used for the estimation of water balance components and for closing the water balance (Andermann et al., 2012; Cochand et al., 2019; Hood and Hayashi, 2015; McClymont et al., 2010). However, closing the water balance may be strongly impaired in small ungauged catchments where the large amount of data required is not satisfied as ground data are rarely available and remote sensing data are often too coarse (Acharya et al., 2021; Hobouchian et al., 2017; Longuevergne et al., 2010; Zambrano-Bigiarini et al., 2017). Besides, addressing the role of geological structures on groundwater flow and surface water-groundwater

interaction implicitly requires the selection of characterization methods that are able to image geological discontinuities, that is, those with a relatively fine resolution (tens of meters). In this context, geophysics has emerged as a non-destructive method to survey the subsurface at various scales and depths and in some occasions hydrogeological processes (Binley et al., 2015; Robinson et al., 2008). Electrical Resistivity Tomography (ERT) has been widely used (Samouelian et al., 2005) for soil moisture studies (Araya Vargas et al., 2021), the identification of groundwater aquifer geometry, and the study of geological structures (Ball et al., 2010; Martos-Rosillo et al., 2019; Robert et al., 2011). ERT cross-sections can be aligned to reveal resistivity contrasts resulting from geological structures and to construct a 3D representation based on previous geological knowledge (Figueroa et al., 2021). Gravity surveys can be performed at different spatial scales, from local to regional, and can identify tiny changes in gravity to obtain structural information (Telford et al., 1990). Gravity surveys are generally used to delineate the basement depth of sedimentary basins (Abbott and Louie, 2000; Figueroa et al., 2021; Murty and Raghavan, 2002; Yáñez et al., 2015); however, they can also be used to identify geological contacts and discontinuities that do not outcrop (Ruelleu et al., 2010). While they can be used to image geological structures, the abovementioned methods and many more geophysical methods are unable to image hydrogeological features without an additional hydraulic-based constraint such as groundwater level, water resurgences, etc. Besides, ground geophysical surveys of mountain catchments are limited by their remoteness, which has raised interest in the use of aerial surveys. So far, aerial geophysical surveys have been conducted by helicopter or airplane for large-scale studies (>1,000 km^2) focusing on major regional geological structures (Dumont et al., 2021; Hussien et al., 2017; Lopez Loera et al., 2015; Reeves, 2005; Vittecoq et al., 2019). Yet, the recent emergence of drones (UAV) has offered a potential means to explore the subsurface framework at much smaller scales and more systematically, thanks to their smaller clearance distances (less than 50 m) and closer profiles.

Hydrogeology is fundamentally at the cross-roads of various disciplines and multidisciplinary approaches have naturally shown their value for characterizing, understanding and managing groundwater as the joint use of various methods makes it possible to more widely cover the parameters space (Kreamer et al., 2021). Regarding mountain catchments, studies based on various methods became essential to develop a more in-depth knowledge of hydrogeological systems and to propose new conceptual models of their hydrogeological functioning (Christensen et al., 2020; Manning et al., 2021; Markovich et al., 2021; Ruiz-Pereira et al., 2023; Somers et al., 2016). However, the choice of data that are informative and complementary enough and the interaction between disciplines that may not share the same approaches and perceptions are in itself challenging. The main objective of this study is to develop a novel multi-disciplinary approach to assess the hydrogeological role of geological features at the catchment scale in ungauged mountain catchments. To do so, we perform a thorough geological characterization through a multiscale geological mapping and ground and aerial geophysical instrumentation to accurately outline both the surface and the subsurface geological framework. To clearly establish the impact of geological features and heterogeneity on hydrogeological structures, hydrogeological information is retrieved from various sources and various data types, including spatially-distributed baseflow measurements, the Normalized Difference Vegetation Index (NDVI), and a thermal spring location and temperature. The multidisciplinary methodology is designed to get a comprehensive understanding of the system and establish a causal link between geological and hydrogeological features which cannot be achieved by each of the methods separately. The scope of this study is functional and pragmatical aiming to identify the key geological structures for groundwater flow but not the entire geological framework and focusing on a key hydrological variable which is the streamflow.

In the following section, we present the application of the methodology to the Parque Nacional del Río Clarillo, an ungauged mountain catchment in Chile whose large geological heterogeneity is illustrative of both the scientific and methodological challenges to the analysis of mountain groundwater systems.

After presenting the results in section 3, we discuss the capacity of various hydrogeological conceptual models to explain the observed streamflow variations and hydric singularities as well as the differentiating aspects and novelty of the proposed approach.

2. Study site and methodology

2.1. Study site

2.1.1. Climatic context

The Parque Nacional del Río Clarillo is an ungauged catchment with an area of 130 km² located 35 km southeast of Santiago (-33.72°, -70.49°, Figure 1 a and b). Situated in a semi-arid climate, the park is suffering from the uninterrupted drought that has been affecting Central Chile since 2010 and had led to a decrease in precipitation of about 30% in this region (Garreaud et al., 2020). Though presenting significant interannual variability, the average annual precipitation downstream of the park historically amounted to approximately 700 mm during the period 1990-2010(DMC, 2023). However, since the beginning of the drought, it very often does not exceed 300 mm and reached 400 mm on very few occasions (DMC, 2023). Accordingly, observations by park rangers and technical studies (Niemeyer, 2002) point at a severe reduction of the Río Clarillo baseflow of close to 75%. Still, these observations should be interpreted with caution as they remain very sparse. The Río Clarillo regime is pluvionival with streamflow maintained by snowmelt in the upper part of the catchment. While snowmelt historically lasted up to the end of March, the past few years have shown an earlier melting, which rarely persists after January according to observations by park ranger.

2.1.2. Geological context

The present-day configuration of the Andes of Central Chile is marked by the development of two margin-parallel ranges, the Coastal Cordillera to the west and the Principal Cordillera to the east, separated by the Central Depression alluvial plain. The study area is located on the western margin of

192 the Principal Cordillera (Figure 1a), and is uplifted by more than 2,000 m over the Central Depression
193 by the cumulative displacement of the west-vergent San Ramón-Pocuro Fault System (SRPFS)(Armijo
194 et al., 2010; Rauld, 2002).

195 The geology of the Río Clarillo catchment records the evolution of the western margin of the Eocene-
196 Miocene Abanico Basin (Figure 1c). This includes the volcanic and sedimentary rocks of the extensional
197 phase of the Abanico Basin, the Abanico Formation (Oligocene-Miocene), and the volcanic rocks that
198 represent the tectonic inversion of the basin, that is, the Miocene Farellones Formation (Charrier et
199 al., 2002). These stratified units are intruded by granitic rocks of the La Obra pluton (c.a. 21 Ma), (Figure
200 1c). However, at the scale of this work, there is no consensus on whether the rock bodies outcropping
201 in the Río Clarillo catchment should be assigned to these formal units (Fock, 2005; Piquer et al., 2021,
202 2017; Thiele, 1980).

203 At the regional scale, the Abanico Formation shows intense deformation of tight west-vergent folds in
204 the westernmost outcrops that gradually decreases towards the east to wide and open folds. The
205 Farellones Formation lies unconformably over the tight folds affecting the Abanico Formation in the
206 westernmost outcrops, showing less intense folding, and becomes gradually parallel to the underlying
207 Abanico formation towards the east (Charrier et al., 2002; Fock, 2005).

208 Scarce Pliocene to Holocene alluvial and fluvial deposits are preserved in the main fluvial valley and in
209 tributary ravines. From the mouth of the Río Clarillo valley, alluvial deposits show a strong increase in
210 thickness towards the Central Depression, reaching a thickness of up to 500 m (González et al., 2018;
211 Yáñez et al., 2015).

212 2.2. Geological methodology

213 The geological survey consisted of a regional geological mapping (1:100,000 scale) of the whole Río
214 Clarillo catchment (Figure 1c), refining the previous geological maps in the area. To assess controls on
215 primary permeability, since there is no consensus on the assignment of these rock units to the formal

lithostratigraphic units in the area (Fock, 2005; Piquer et al., 2021; Thiele, 1980), strictly lithological units were defined and mapped. As for the controls on structural features on secondary permeability, faults, folds, and fracture zones were surveyed at a finer scale, focusing on fracture systems along the riverbed and on hilltops where rock outcrops are observed.

2.3. Geophysical methods

The geophysical study involves the joint use of a UAV-based aeromagnetic system (with only limited previous applications in the Andes (Sanhueza et al., 2022; Yáñez et al., 2020)) and on-ground transect data obtained from ERT and gravimetry. As shown in Figure 1c, transect (A-A') and the drone coverage are oriented east-west to perpendicularly intersect the main structures present in the study site as the SRFPS is N-S oriented (see section 2.1.2 for a description of the geological context). As shown in Figure 1c, a second roughly E-W transect (B-B') is also performed. This transect is located 10 km northeast of the Río Clarillo catchment, in the Río Coipo valley, and was performed to gain insights on the geological structures on the eastern flank of the La Obra pluton, where the rough topography prevents the use of ground-based geophysical methods along the primary transect A-A'. Furthermore, having two parallel profiles allows a 3D view of the geology to be obtained (N-S along strike variations). We use the same methodological approach in both transects. The results of this second transect are presented in the supplementary material; nevertheless, their contribution to our geological interpretation of the study area is included in the discussion.

2.3.1. Electrical Resistivity

Electrical Resistivity Tomography is an exploration method that measures the subsurface distribution of electrical resistivity with high resolution (Dahlin, 2001). It can be used to detect water-saturated areas and the depth of the contact between the sediment surface layer and the basement unit, as well as to identify fracture and fault zones in the basement unit, which show lower resistivity compared to

239 the surrounding unfractured rock. As the ERT method has optimal definition in the shallow subsurface,
240 it is limited to depths of around 250-300 m, depending on the dipole separation.

241 Data were acquired using an ABEM Terrameter LS2 (Guideline Geo, Stockholm, Sweden). The
242 measurement protocol involved a Dipole-Dipole array with 48 electrodes and a 20 m inter-electrode
243 spacing. Each profile was 1 km long with an investigation depth of about 250-350 m. The Dipole-Dipole
244 array was chosen for its particularly good definition of the vertical structures typically present in faults
245 and geological layers (Loke, 2004; Samouelian et al., 2005).

246 The Río Clarillo and Río Coipo transects are respectively composed of six and seven profiles (the former
247 having fewer profiles due to field conditions). Both profiles present a 500 m overlap between each
248 profile to obtain a better characterization of the structures. The apparent resistivity datasets obtained
249 in the field for each profile were inverted separately to obtain 2D resistivity cross-sections. The data
250 were inverted using the ZonRes2D software (Kaminsky, 2010). Each profile was then "stitched" to the
251 adjacent one to obtain the full transect using the stitching tool in the Oasis Montaj software (Seequent,
252 Christchurch, New Zealand). This stitching method is necessary to obtain the full-length transect
253 without noticeable edge effects at the extremes of the profiles.

254 2.3.2.Gravimetry

255 Gravimetry measures the gravity field caused by differences in mass distribution below the surface.
256 Variations in the residual gravity anomaly i.e. the difference between properly corrected gravity
257 observations and the regional field (see a description of this process later in this section) can be
258 indirectly associated with the subsurface density distribution, which can in turn be used to infer
259 geological information along the measured profile. We used a CG-5 Autograv relative gravimeter
260 (Scintrex, Concord, ON, Canada) with a resolution of 5 µGal and a Trimble R4 GNSS (Trimble,
261 Westminster, CO, USA) receiver that gives the position and altitude with a precision of less than 30 cm.
262 The Río Clarillo transect (A-A') has 56 gravimetric stations spaced ≈50 m apart along a 2.5 km long

263 profile (Figure 1c). The Río Coipo transect (B-B') presents 72 gravimetric stations spaced ≈100 m apart
264 along a 7 km long profile (Figure 1c).

265 Gravity data were corrected using standard procedures (Telford et al., 1990): (1) The tidal correction
266 is computed by the instrument during all the measurements and the drift correction is estimated as a
267 linear function during the day with measurements at the base station at the beginning and end of the
268 day; (2) The latitude correction was computed using the WGS84 reference ellipsoid; (3) The absolute
269 gravity value was obtained using the base station at the Department of Geophysics of the University
270 of Chile (Universidad de Chile) (Gravity DGF: 979,416.07 [mGal]); (4) The Free-air and Bouguer
271 corrections were computed using the altitude obtained from the differential GNSS and assuming a
272 mean subsurface density of 2.67 g/cm^3; and (5) The Terrain correction was calculated with a high-
273 resolution digital terrain model with a 5 m resolution (AW3D Standard product, acquired from NTT
274 DATA Corporation). Finally, the regional effect was removed to obtain the residual anomaly along the
275 profile due to the effect of the low-density bodies under the Principal Cordillera at deeper crustal
276 levels: for this purpose, the Bouguer anomaly of Santiago obtained by Yáñez et al. (2015) was removed
277 from our data. Then, the result was processed using the rock measurement performed at a point of
278 zero-anomaly as a constraint. After correcting the gravity observations, we obtained a residual gravity
279 anomaly suitable for geologically constrained gravity modelling. The modelling process consisted of a
280 forward modelling using the ModelVision software (Encom), with the model output being compared
281 to the residual gravity anomaly.

282 2.3.3.UAV-based magnetic survey

283 In the magnetic method, the magnetic properties of rocks are measured using a magnetometer. It
284 provides a valuable tool to map geology and structural networks if they involve magnetic contrasts.
285 The operational simplicity of total field magnetometers, in which the magnetic field is recorded almost
286 instantaneously regardless of the sensor or platform orientation, make them very suitable for use in
287 mobile platforms, such as airplanes, ships, or UAVs. We used a Bartington MAG03 fluxgate

magnetometer (Bartington Instruments, Oxon, United Kingdom) with three orthogonal components mounted on a UAV system. We surveyed one block (see spatial distribution in Figure 1c, purple polygon). The polygon is 6,600 m long and 1,800 m wide, covering large parts of the reserve and both side contacts of the intrusive unit. Lines were flown in the N-S direction with a line separation of 200 m and a flight altitude of 50-80 m above terrain level. The location was recorded with a standard GPS with an accuracy of 5m.

The following corrections were applied to the raw magnetic field observations: (1) removal of diurnal variations; (2) removal of the Earth's magnetic field (IGRF, International Geomagnetic Reference Field); and (3) recovery of the total magnetic field from the three-component fluxgate magnetometer (for details see Sanhueza et al., (2022)). After data correction, we obtained a residual magnetic field dominated by magnetic sources in the shallow crust. The data were then reduced to the magnetic pole (RTP), an approach which aims to centre anomalies over their source (Blakely, 1995). The magnetic data were then interpreted qualitatively by comparing the RTP map with geological, hydraulic, and additional geophysical information.

2.4. Streamflow measurements, remote sensing data, and hydric markers

The Streamflow rate was measured from the outlet of the national park up to the confluence of the two main tributaries of the Río Clarillo, 9 km further upstream (Figure 1b). The measurements were carried out at least every kilometre and when possible at smaller intervals in the sectors of interest, that is, where the flow exhibited significant variation. Data were acquired with an Acoustic Doppler Velocimeter (FlowTracker, SonTek). Three campaigns were completed during the 2019 recession period (austral autumn) to better evidence the contribution of groundwater to the baseflow. The first and third campaigns are complete campaign from the outlet P0 to the confluence P8 while the second campaign is simply a small-scale campaign between points P4 and P5. If the streamflow measurements can be quantitatively compared between each campaign, the three campaigns exhibit similar trends

and features and can serve as cross-validation. Some data points are missing due to technical, logistical or staff complications on site (e.g., point P5 during the third campaign). We also considered different types of soft hydric data (i.e., qualitative data), which are essential in ungauged catchments (Seibert and McDonnell, 2015). The soft data were mainly obtained from the knowledge of the nearby community of Pirque, the testimony of park rangers, and the authors' observations during field campaigns.

To complement the streamflow analysis and to obtain a long-term assessment of the streamflow dynamics and the persistence of possible resurgence zones, we analysed NDVI time series. The NDVI measures the difference between infrared and red light to quantify vegetation presence and density using reflectance bands. It is the most common index used in remote sensing to understand drought processes (Gu et al., 2008, 2007), related plant water stress (Ballester et al., 2019; Katsoulas et al., 2016), and to evaluate groundwater fluctuation and vegetation cover (Pan et al., 2008; Seeyan et al., 2014). The NDVI was obtained from the MODIS/MCD43A4 product (Schaaf and Wang, 2015) through the Google Earth Engine (Gorelick et al., 2017) from 24 Feb 2000 to 31 Dec 2019, that is, covering the drought period and the previous decade.

2.5. Conceptual hydrogeological models

We develop various conceptual hydrogeological models and discuss hypotheses in relation to the streamflow evolution through the catchment. As argued later in section 3.4, the groundwater-surface water interaction is highly likely to be related to geological discontinuities. Geological controls on groundwater-surface water interaction are further reinforced by a parallel sensitivity study (not shown here) of baseflow evolution through the catchment to varying uniform recharge rates on homogeneous numerical models in which topography-driven groundwater flows do not reproduce the streamflow measurements carried out in our catchment. Therefore, the conceptual models differ mostly in terms of the drainage surfaces and geological structures involved in the groundwater-surface

water interaction. The conceptual models are presented in detail in section 4.1 following the joint interpretation of data presented in section 3.4.

To offer a more quantitative point of view, the proposed conceptual models can be segregated by simple mass balance. Assuming steady-state conditions with no storage in the soil nor in the aquifer, a relatively low direct runoff coefficient considering the forest cover and relatively constant baseflow over the year, the effective precipitation in each catchment (defined as total rainfall minus actual evapotranspiration) can be directly compared to the baseflow per drainage area, *i.e.,* what goes in goes out. A mean yearly value for effective precipitation is estimated from ground-based meteorological data for the period 1985-2013, as acquired by the park administration in the vicinity of the catchment outlet P0 (Figure 1). The estimated effective precipitation over the catchment in this period is close to 120 mm.

3. Results

We successively present the results of the geological mapping for hydrogeological considerations, the geophysical results, and the results related to streamflow measurements and remote sensing analysis.

3.1. Geology

Strictly based on lithological characteristics (Figure 1c), four rock units were defined and mapped in the studied area, some of which were recognized in more than one stratigraphic position. The first is an “Andesitic unit” composed mainly of andesitic lava flows and hypabysal porphyritic intrusives, with minor andesitic tuffs and sandstones. This unit was recognized west of the newly identified Papagayo fault presented in the next paragraph and at the base and in the middle of this fault hanging wall. The second is a “Sedimentary unit”, which is a sandstone-dominated unit that also includes conglomerate, lithic tuff, and andesite intercalations and crops out discreetly in the footwall of the Papagayo fault - extensively in the middle section of its hanging wall and as a small wedge within its upper section. The

359 third is a stratified “Dacitic unit”, which is composed of brightly coloured dacitic lavas and tuffs
360 recognized in the upper section of the Papagayo fault hanging wall. The fourth unit is a “Granitic unit”
361 composed of monzogranites, syenogranites, and granodiorites, which outcrops in the western flank of
362 the Principal Cordillera, intruding the stratified volcanic and sedimentary rocks.

363 The structural features of the study area allow the recognition of two distinct structural domains. The
364 first is a western domain limited by the main trace of the west-vergent San Ramón fault and a newly
365 identified N-S reverse fault, which here is called the Papagayo fault (Figure 1c). This domain shows
366 tight short-wavelength (2-4 km) folds and minor inverse faults, generating highly dipping strata. The
367 second domain is located to the east of the Papagayo fault and shows low dips on the flanks of long-
368 wavelength (6-8 km) folds. However, 2 km east of the Papagayo fault, a west-vergent anticline is
369 recognized in the hilltops affecting the andesitic and sedimentary units. Directly beneath the anticline,
370 faulting and fracturing is recognized affecting the granitic rocks outcropping along the riverbanks. A
371 detailed structural survey in this area showed a zone with a high fracture density with vertical and
372 closely spaced NS- and EW- striking sets and minor inclined NW- and NE-striking sets (criss-crossed
373 zone in Figure 1c).

374 3.2. Geophysical study

375 Figure 2 presents the magnetic field reduced to the magnetic pole. The advantage of this
376 representation is that it tends to show a direct correlation between the magnetic anomaly and the
377 causative magnetic source (i.e., a positive correlation when the magnetic source is more magnetic than
378 the surroundings, and a negative correlation for the opposite case). On this map, we identify four
379 zones, mainly oriented north-south. Going from west to east, the first 2,000 m of the profile (zone 1)
380 presents a strong positive magnetic anomaly that is relatively homogenous in the NS direction. Inside
381 this zone, a short-wavelength (less than 200 m) but persistent negative anomaly is observed at
382 longitude 361,000E. Secondly, in zone 2, between 362,000E and 364,000E, we observe a negative

anomaly with its larger amplitude in the northern half, and tapering off southward. This broad negative domain is followed to the east by another negative domain (zone 3) of the same length and signal amplitude (-60 to -80 nT) but decreasing southward and westward. The limit between zone 2 and zone 3 is a fairly linear positive NS anomaly around 364,000E. Finally, zone 4 extends east of 366,000E, and is characterized by a broad positive anomaly that seems to extend beyond the study area.

In agreement with the geological map, the mineralogical composition of geological units and susceptibility samples taken from outcrops (Table 1), the magnetic sources associated with zones 1 and 4 represent volcano-sedimentary units, with mid-to-high contents of ferromagnetic minerals. In contrast, the negative magnetic anomaly of zones 2 and 3 can be associated with the intrusive body mapped in the geology. This intrusive has a consistently more felsic mineralogy and low magnetic susceptibility with a clear negative contrast compared with the volcanic units in the flanking domains (Table 1). The sharp transition between magnetic zones 3 and 4 can be associated with the mapped contact between the intrusive unit and the volcanic unit at the eastern border of the intrusion. Meanwhile, at the western limit of the study area, we can identify a similarly sharp transition between zones 1 and 2, in good agreement with the contact between the intrusive and volcanic rocks. We postulate that the positive anomaly at 364,000 E (which separates zones 2 and 3) represents a fault that provided room for the emplacement of more mafic magmatism (the andesites of the flanking zones 1 and 4) and/or a path for hydrothermal circulation and secondary magnetic enhancement due to contact metamorphism. This anomaly is hence associated to the newly identified Papagayo fault which appears to be a large-scale regional fault according to the gravimetric survey carried out in the Río Coipo catchment. Looking at the path of the river entering zone 2 going west, we see a change in direction from E-W to S-N, which may be another sign of the influence of this fault on the river network. Finally, in zone 1, the relative negative anomaly at 361,000E may be related to a demagnetization of the volcanic rocks caused by the hydrothermal fluid circulation at the piedmont fault zone.

The Río Clarillo ERT profile (Figure 3) can be separated into two well-defined zones, identified as zones 1 and 2 on the aeromagnetic map. Zone 1 is defined at distances of between 0-1,300 m along the profile, where the environment is much more conductive than the other part of the profile (100-500 ohm.m versus more than 1,000 ohm.m eastward). In this zone there are some small-wavelength heterogeneities (100-200 m) that are relatively positive and tabular (along-profile distances of 200-400 m and 800-1,000 m) and a shallow sub-horizontal negative anomaly (along-profile distance of 100-500 m). Magnetic zone 2 is partially represented between 1,300 – 3,600 m on the ERT profile. It contains a shallow (~ 50 m depth), almost continuous and relatively conductive layer (<300 ohm-m) above a resistant body (> 1,000 ohm-m).

The geological interpretation is based on the locations of the two aeromagnetic zones. The higher resolution of the ERT profile compared to the magnetic data suggest the presence of a shallow layer of sediments overlying the volcanic and intrusive units. Zone 1 evidences a more conductive layer which likely represents the alluvions that cover the volcanoclastic rocks of the western flank of the study area. The magnetic signal in this zone cannot be used to discriminate this sedimentary unit, probably due to its low magnetic content. The vertical conductive structure between 400-500 m and the horizontal thin layer between 0-400 m are likely to be associated with the location of the thermal spring, as this really low resistivity can be associated with saturated sediments. Zone 2, between distances of 1,300 and 3,600 m the eastern portion of the ERT profile, occurs within the granitic intrusion and is covered by a thin layer of alluvial material. The high and rather homogeneous resistivity underneath the thin conductive cover suggests that this intrusive is a relatively homogeneous unit that is probably cut by structures at distances of 2,000 m and 2,800 m along the ERT profile. Even though no regional large-scale structures are defined in this area, Piquer et al. (2021) observed and mapped secondary structures inside the granitic intrusion at similar locations, which supports our working hypothesis on the discontinuity of the granitic body. These results indicate that

these heterogeneities represent faults or fold axes in the geology associated with the domain of high electrical resistivity.

The gravity anomaly along the Río Clarillo valley transect (Figure 4 upper panel) shows two distinctive sectors, a western sector characterized by a relative negative anomaly (-5 mGal) between distances of 0-500 m along the profile. To the east is a wide zone with a relatively steep gradient (2 mGal/km) between distances of 500-1,500 m along the profile. The remainder of the profile, between distances of 1,500-3,500 m, shows a relatively flat gravimetric response at -2.5 mGal. The proposed density model considers a background density of 2.67 gr/cc, as well as the structures and layers defined at the subsurface by ERT and magnetic interpretations. Densities for intrusive and volcanic rocks are based on in-situ rock sample measurements (Table 1), while sediment density is obtained from Yáñez et al. (2015).

As shown in Figure 4 upper panel, the model response is in good agreement with observations, and is thus a plausible solution that is consistent with geological observations. Low density and thick sedimentary cover above the volcanic basement explain the lower gravity of the western side. The thickness of the sedimentary unit decreases eastward in line with the decrease of the amplitude in the negative gravity signal. This sedimentary body represents the alluvial fan at the piedmont. Considering the interpretation of the ERT profile, the low-resistivity zone at a distance of around 500 m is here represented as a fractured area in the volcanic unit and a low-density area in the sediment layer (1.85 gr/cc). As seen on the ERT profile as a low-resistivity zone (below 50 ohm.m), this low-density zone extends between distances of 0 and 400 m, in the sediment layer, and probably represents a clay-dominated body associated with the thermal spring zone recognized in the area. Towards the east (zone 2), an almost flat signal is modelled as the gravimetric response of the more felsic intrusive body (2.63 gr/cc) covered by a relatively thin layer of sediments. In this zone, the sediment cover is approximately 50 m, which agrees well with the ERT transect, which shows a covering of intermediate-resistivity material of a similar thickness. At the contact between the two zones, at a distance of around

1,300 m, there is a small decrease in the gravity anomaly. This negative anomaly is associated with a low-density fractured zone. This contact zone is associated with the fractures induced by the intrusive emplacement. The fracture zone identified at a distance of 500 m could favour groundwater exfiltration, creating a preferential upwelling flow, according to the location of the thermal spring over this fault. The proximity of the two fracture zones (which are located at along-profile distances of 500 m and 1,300 m) and their similar vertical structure indicate that a joint fault system may be connected at depth and act as listric faults.

3.3. Streamflow measurements and remote sensing analysis

Streamflow measurements acquired during the 2019 recession are displayed with regards to drainage (or upslope) area (Figure 5). A few interesting features are observed. First, we observe a significant increase of the streamflow at point P1 (grey triangles in Figure 5). However, this increase is not systematically observed within the same recession period (orange squares in Figure 5). Second, and most notably, it exhibits a significant increase of approximately 50% within a 1km distance (between P5 and P4-P3). We interpret this variation as groundwater exfiltration as there is no significant increase of the drainage area and there is no affluent observed in the area or a superficial supply of any type (snowmelt, water bodies). Groundwater exfiltration has been observed in the Carrizal area (Figure 1c) by park rangers, who have noted that “water is usually seen disappearing in the river” while they are going back up the Río Clarillo which is consistent with the lower streamflow rate from P4 to P5. Additionally, some hydric features are observed downstream of point P5, such as a permanent puddle about 50 m uphill and a curtain of dripping water on the east at the riverbank.

The persistency of the groundwater exfiltration is confirmed by the difference in NDVI between the Carrizal area and the entire national park. The Carrizal area is displayed here as a strip 1,000 m in length and 500 m in width along the east side of the river where geological and hydric features have been observed. Over the period 2000-2019, the mean NDVI in the Carrizal area was 0.57, while it was 0.36

in the entire national park. The difference in NDVI between the Carrizal area and the entire national park is almost systematically positive (Figure 6), indicating that the Carrizal area has denser vegetation due to a higher water availability. In conclusion, both qualitative observations and quantitative data indicate that the groundwater exfiltration between P5 and P4 has persisted for at least the last two decades.

3.4. Joint interpretation of geophysical and geological results and hydraulic markers

The interpretation of the magnetic map allows us to describe four north-south zones. The ERT and the gravity transects overlap zones 1 and 2 and indicate a similar spatial extent of these zones, which reinforces our results and interpretations. Moreover, the thermal spring is identified using each of the geophysical methods, indicating a relationship between this feature and the presence of a fault inside the volcanic unit. The temperature of the thermal spring is about 23°C. As the geothermal gradient is about 3°C/100 m in this region (Muñoz and Hamza, 1993; Valdenegro et al., 2019), it is possible to approximate at first order that this thermal source is fed along a 300 m deep structure at least, which is supported by the ERT interpretation and the gravity modelling. Both methods indicate that the thermal spring is likely associated to upwelling flow along a fault or fractures zone as seen on other locations along the Andes in Central Chile (Figueroa et al., 2021). Our second hydraulic indicator is the increase of baseflow that was measured between points 5 and 4. This area was only monitored with a UAV-based magnetic study. The contact between the volcanic unit at the eastern end of the reserve and the intrusive unit might be of significance for the increase of the river baseflow. Nevertheless, the location of the increase in the river flow is not exactly located over the contact defined on the aeromagnetic map (Figure 2). According to the geological map, the resurgence area close to the contact, presents a pattern of local east-west fractures (criss-crossed zone in Figure 1c). As seen at the

503 western edge of the contact between the intrusive unit and the volcanic unit (Figure 4), a highly
504 damaged zone engenders the structural control of water flows.

505

506 4. Discussion

507 Based on the various observations described in the previous section, we first discuss the capacity of
508 various conceptual hydrogeological models to explain the observed streamflow variations and hydric
509 singularities. We then discuss the differentiating aspects and novelty of the proposed multi-disciplinary
510 approach for characterizing groundwater flow patterns in mountain catchments and for identifying
511 structural controls on groundwater flow patterns and surface water–groundwater interaction.

512 4.1. Conceptual hydrogeological models

513 We propose three different conceptual models based on the observed geological features. First,
514 groundwater exfiltration between P5 and P4-P3 could simply originate from the local drainage of
515 lateral hillslopes in the Carrizal area, which are partly composed of alluvial deposits (Model 1 of Table
516 2, Figure 7). However, the Carrizal area offers a very small drainage area (3 km^2 from P4 to P5 and 9
517 km^2 from P3 to P5), which we argue is likely insufficient to explain the full extent of the resurgence.
518 Second, as the exfiltration occurs in the vicinity of the contact between the intrusive and volcanic units,
519 it could be related to a reduction of the groundwater seepage area, that is, a reduction of the active
520 depth of the system due to a much less permeable underlying unit outcropping (Model 2 of Table 2,
521 Figure 7), consistent with the results from section 3.2. In that case, the drainage area could be the
522 entire catchment area upstream of point P5, which is close to 100 km^2. Finally, as shown on the
523 geological map (Figure 1c) and described in section 3.1, the Carrizal area shows a large number of
524 heterogeneities inside the intrusive unit. It is described as highly fractured in relation to a local E-W
525 steeply dipping fault zone (criss-crossed zone in Figure 1c) and close to the N-S major Papagayo fault

526 This local fault zone and the associated water resurgence may be a local effect of the E-W faults and
527 the fracture network in this area with no influence of regional structures. Still, it is likely that the
528 principal N-S structure is directly related to these E-W faults forming a fault network with secondary
529 structures perpendicular to the major one. Supporting evidence for this last model is provided by the
530 very low streamflow from the nearest downstream tributary, Los Bueyes (green catchment in Figure
531 7), with no significant streamflow increase measured at P2. The catchment contributing to this
532 tributary is directly stroke by the N-S fault identified by both the geological mapping and UAV-based
533 magnetic results. This N-S structure likely exports groundwater of the contributing subcatchment to
534 the identified resurgence area (Model 3 of Table 2, Figure 7).

535 As presented in Table 2 and above, each conceptual model corresponds to significantly different
536 drainage areas. Model 2 can be discarded as the estimated flow from simple mass balance (as
537 presented in section 2.5) is seven times larger than the resurgence flow. In model 1 and model 3, the
538 estimated flow is 0.22 and 0.90 times the resurgence flow, respectively. Thus, model 3 is the most
539 likely scenario considering the drainage area of each sub catchment. Hypothetically, a combination of
540 models 1 and 3 might as well explain the resurgence processes considering the uncertainty in the
541 simple hydrological balance presented in section 2.5.

542 4.2. Differentiating aspects and novelty of the approach

543 This work presents a methodology to identify structural controls on groundwater flow patterns and
544 surface water–groundwater interaction. The scope of the methodology is above all functional in the
545 sense that it aims to identify the key geological structures for groundwater flow but in no way to
546 characterize the entire geological framework. This functional scope necessarily impacts the scale of
547 the study which is neither at the fault scale (for example, there is no topological analysis of the faults
548 zone), nor at the catchment scale as the elementary bulk unit. This functional scope besides impacts
549 the methodological choices made, following the informational content of well-known data and

technics. As the current approach aims at linking geological structures to hydrogeological structures, it is inevitable to acquire hydraulic-related data. For that aspect, widely-used methods based on dissolved elements (environmental tracers, water isotopes, hydrogeochemistry) are directly related to transport processes and hence to groundwater flow and hydraulic gradient. However, their inability to clearly identify local scale processes mainly due to mixing, limits their use when addressing problems related to groundwater flow architecture as it is the case here. On the contrary, baseflow measurement is an easily accessible data that can be related to local flow processes as the resolution of spatially-distributed measurements can be arbitrary fixed. Beyond this consideration, streamflow is a variable of interest in various disciplines including hydroecology. In that sense, the comprehensive methodology proposed here could be easily extended to hydroecology or hydrobiology.

The novelty of the proposed methodology lies mainly in the innovative implementation of classical methods from various disciplines that are conjointly designed and iteratively carried out. The geological study has been indeed conducted at multiple scales: at a traditional main scale (1:100,000) and at a finer scale to incorporate some elements (e.g., the N-E secondary fracture zone) that would confirm hydraulic observations. It results in a hybrid geological map partly fed by hydrogeological considerations. Regarding geophysical surveys, they significantly compliment the multiscale geological mapping. The inclusion of a second geophysical transect in the north of the study area (transect B-B' n Figure 1c) confirms the general N-S orientation and regional scale of some structures (results presented in supplementary material). Meanwhile, the UAV-based magnetic study, performed here at high-resolution in comparison to previous studies, does not only provide valuable information in remote areas but also constitutes a unifying method allowing the creation of a coherent geological model thanks to its fast and large covering.

Finally, while spatially-distributed streamflow campaigns are not commonly used in hydrology, they have shown here to be valuable to identify and confirm critical features of the baseflow evolution within the catchment. If spatially-distributed flow measurements may seem tedious, low-cost

instrumentation and recently-developed optical methods could allow a systematization of measurements.

5. Conclusions

We propose a comprehensive methodology to unravel geological controls on groundwater flow and surface water-groundwater interaction in mountain catchments. Geological mapping, on-ground and aerial geophysics, and hydraulic data are acquired to simultaneously image geological structures and their hydrogeological manifestations.

Using the novel methodology, we identify peculiar hydric behaviours in an ungauged Andean catchment, including a significant and localized groundwater exfiltration that seems to be imported from a neighbouring subcatchment and related to the presence of a regional N-S fault and a secondary set of E-W local faults.

The novelty of the methodology mainly lies in the innovative implementation of classical methods: multi-scale geological mapping, spatially distributed streamflow measurements, high-resolution aerial geophysics. This novel methodology is distinguished by its pragmatism in that it focuses on the geological structures that are the most significant for flow without aiming to characterize the entire geological framework.

The findings have significant implications for the management and monitoring of the study site as flow singularities such as the abrupt streamflow change that may strongly affect the biogeochemical conditions in the river, like biogeochemical hotspots.

6. Acknowledgments

This study received financial support from the project ANID-Conicyt/Fondecyt de Iniciación n°11170380. The authors would like to thank the Pirque community for their incredible kindness, their constant support and their interest in the *HydroPirque* project. Miles y miles de gracias a la CONAF: Don Carlos, Don Luis P., Don Luis C., Doña Catalina y todos los guardaparques de la reserva. Miles de gracias también al comité de Agua Potable Rural El Principal: a la señora Nora y a Erik, a la municipalidad de Pirque y a Nicolas. Thanks to Mr. Carlos Uribe del Río Coipo: sometimes research hangs by a thread, or rather by a padlock key. The authors are thankful to the two anonymous reviewers and the associated editor for their fruitful comments that significantly improved the manuscript.

7. References

Abbott, R.E., Louie, J.N., 2000. Depth to bedrock using gravimetry in the Reno and Carson City, Nevada, area basins. Geophysics 65, 340–350. https://doi.org/10.1190/1.1444730

Acharya, B.S., Bhandari, M., Bandini, F., Pizarro, A., Perks, M., Joshi, D.R., Wang, S., Dogwiler, T., Ray, R.L., Kharel, G., Sharma, S., 2021. Unmanned Aerial Vehicles in Hydrology and Water Management: Applications, Challenges, and Perspectives. Water Resources Research 57. https://doi.org/10.1029/2021WR029925

Alvarez-Campos, O., Olson, E.J., Welp, L.R., Frisbee, M.D., Zuñiga Medina, S.A., Díaz Rodríguez, J., Roque Quispe, W.R., Salazar Mamani, C.I., Arenas Carrión, M.R., Jara, J.M., Ccanccapa-Cartagena, A., Jafvert, C.T., 2022. Evidence for high-elevation salar recharge and interbasin groundwater flow in the Western Cordillera of the Peruvian Andes. Hydrol. Earth Syst. Sci. 26, 483–503. https://doi.org/10.5194/hess-26-483-2022

Andermann, C., Longuevergne, L., Bonnet, S., Crave, A., Davy, P., Gloaguen, R., 2012. Impact of transient groundwater storage on the discharge of Himalayan rivers. Nature Geosci 5, 127–132. https://doi.org/10.1038/ngeo1356

Araya Vargas, J., Gil, P.M., Meza, F.J., Yáñez, G., Menanno, G., Garcia-Gutierrez, V., Luque, A.J., Poblete, F., Figueroa, R., Maringue, J., Perez-Estay, N., Sanhueza, J., 2021. Soil electrical resistivity monitoring as a practical tool for evaluating irrigation systems efficiency at the orchard scale:

a case study in a vineyard in Central Chile. Irrig. Sci. 39, 123–143. https://doi.org/10.1007/s00271-020-00708-w

Armijo, R., Rauld, R., Thiele, R., Vargas, G., Campos, J., Lacassin, R., Kausel, E., 2010. The West Andean Thrust, the San Ramón Fault, and the seismic hazard for Santiago, Chile. Tectonics 29, n/a-n/a. https://doi.org/10.1029/2008TC002427

Ball, L.B., Ge, S., Caine, J.S., Revil, A., Jardani, A., 2010. Constraining fault-zone hydrogeology through integrated hydrological and geoelectrical analysis. Hydrogeol. J. 18, 1057–1067. https://doi.org/10.1007/s10040-010-0587-z

Ballester, Brinkhoff, Quayle, Hornbuckle, 2019. Monitoring the Effects of Water Stress in Cotton using the Green Red Vegetation Index and Red Edge Ratio. Remote Sensing 11, 873. https://doi.org/10.3390/rs11070873

Baraer, M., McKenzie, J., Mark, B.G., Gordon, R., Bury, J., Condom, T., Gomez, J., Knox, S., Fortner, S.K., 2015. Contribution of groundwater to the outflow from ungauged glacierized catchments: a multi-site study in the tropical Cordillera Blanca, Peru. Hydrol. Process. 29, 2561–2581. https://doi.org/10.1002/hyp.10386

Barnett, T.P., Adam, J.C., Lettenmaier, D.P., 2005. Potential impacts of a warming climate on water availability in snow-dominated regions. Nature 438, 303–309. https://doi.org/10.1038/nature04141

Beniston, M., 2003. Climatic change in mountain regions: A review of possible impacts. Clim. Change 59, 5–31. https://doi.org/10.1023/A:1024458411589

Bense, V.F., Gleeson, T., Loveless, S.E., Bour, O., Scibek, J., 2013. Fault zone hydrogeology. Earth-Science Reviews 127, 171–192. https://doi.org/10.1016/j.earscirev.2013.09.008

Binley, A., Hubbard, S.S., Huisman, J.A., Revil, A., Robinson, D.A., Singha, K., Slater, L.D., 2015. The emergence of hydrogeophysics for improved understanding of subsurface processes over multiple scales. Water Resour. Res. 51, 3837–3866. https://doi.org/10.1002/2015WR017016

Bishop, K., Buffam, I., Erlandsson, M., Folster, J., Laudon, H., Seibert, J., Temnerud, J., 2008. Aqua Incognita: the unknown headwaters. Hydrol. Process. 22, 1239–1242. https://doi.org/10.1002/hyp.7049

Blakely, R.J., 1995. Potential Theory in Gravity and Magnetic Applications, 1st ed. Cambridge University Press. https://doi.org/10.1017/CBO9780511549816

Brunner, P., Cook, P.G., Simmons, C.T., 2009. Hydrogeologic controls on disconnection between surface water and groundwater. Water Resour. Res. 45. https://doi.org/10.1029/2008WR006953

Caine, J.S., Evans, J.P., Forster, C.B., 1996. Fault zone architecture and permeability structure. Geology 24, 1025–1028. https://doi.org/10.1130/0091-7613(1996)024<1025:FZAAPS>2.3.CO;2

Charrier, R., Baeza, O., Elgueta, S., Flynn, J.J., Gans, P., Kay, S.M., Muñoz, N., Wyss, A.R., Zurita, E., 2002. Evidence for Cenozoic extensional basin development and tectonic inversion south of the flat-

slab segment, southern Central Andes, Chile (33°–36°S.L.). Journal of South American Earth Sciences 15, 117–139. https://doi.org/10.1016/S0895-9811(02)00009-3

Christensen, C.W., Hayashi, M., Bentley, L.R., 2020. Hydrogeological characterization of an alpine aquifer system in the Canadian Rocky Mountains. Hydrogeol J 28, 1871–1890. https://doi.org/10.1007/s10040-020-02153-7

Clarke, A., Mac Nally, R., Bond, N., Lake, P.S., 2008. Macroinvertebrate diversity in headwater streams: a review. Freshw. Biol. 53, 1707–1721. https://doi.org/10.1111/j.1365-2427.2008.02041.x

Cochand, M., Christe, P., Ornstein, P., Hunkeler, D., 2019. Groundwater Storage in High Alpine Catchments and Its Contribution to Streamflow. Water Resour. Res. 55, 2613–2630. https://doi.org/10.1029/2018WR022989

Condon, L.E., Maxwell, R.M., 2015. Evaluating the relationship between topography and groundwater using outputs from a continental-scale integrated hydrology model. Water Resour. Res. 51, 6602–6621. https://doi.org/10.1002/2014WR016774

Cuthbert, M.O., Gleeson, T., Moosdorf, N., Befus, K.M., Schneider, A., Hartmann, J., Lehner, B., 2019. Global patterns and dynamics of climate–groundwater interactions. Nature Clim Change 9, 137–141. https://doi.org/10.1038/s41558-018-0386-4

Dahlin, T., 2001. The development of DC resistivity imaging techniques. Comput. Geosci. 27, 1019–1029. https://doi.org/10.1016/S0098-3004(00)00160-6

DMC, 2023. Dirección Meteorológica de Chile [WWW Document]. https://climatologia.meteochile.gob.cl/. URL (accessed 12.12.22).

Dumont, M., Reninger, P.A., Aunay, B., Pryet, A., Jougnot, D., Join, J.L., Michon, L., Martelet, G., 2021. Hydrogeophysical Characterization in a Volcanic Context From Local to Regional Scales Combining Airborne Electromagnetism and Magnetism. Geophysical Research Letters 48. https://doi.org/10.1029/2020GL092000

Egan, P.A., Price, M.F., 2017. Mountain ecosystem services and climate change: A global overview of potential threats and strategies for adaptation.

Fan, Y., 2019. Are catchments leaky? WIREs Water 6. https://doi.org/10.1002/wat2.1386

Figueroa, R., Viguier, B., Taucare, M., Yáñez, G., Arancibia, G., Sanhueza, J., Daniele, L., 2021. Deciphering groundwater flow-paths in fault-controlled semiarid mountain front zones (Central Chile). Sci. Total Environ. 771, 145456. https://doi.org/10.1016/j.scitotenv.2021.145456

Fleckenstein, J.H., Krause, S., Hannah, D.M., Boano, F., 2010. Groundwater-surface water interactions: New methods and models to improve understanding of processes and dynamics. Advances in Water Resources 33, 1291–1295. https://doi.org/10.1016/j.advwatres.2010.09.011

Fock, A.I., 2005. Cronología y tectónica de la exhumación en el neógeno de Los Andes de Chile Central entre los 33° y los 34° S. Tesis geólogo--Universidad de Chile., Santiago de Chile.

Freeman, M.C., Pringle, C.M., Jackson, C.R., 2007. Hydrologic connectivity and the contribution of stream headwaters to ecological integrity at regional scales. J. Am. Water Resour. Assoc. 43, 5–14. https://doi.org/10.1111/j.1752-1688.2007.00002.x

Garreaud, R.D., Boisier, J.P., Rondanelli, R., Montecinos, A., Sepúlveda, H.H., Veloso-Aguila, D., 2020. The Central Chile Mega Drought (2010–2018): A climate dynamics perspective. Int J Climatol 40, 421–439. https://doi.org/10.1002/joc.6219

Ginn, T.R., Haeri, H., Massoudieh, A., Foglia, L., 2009. Notes on Groundwater Age in Forward and Inverse Modeling. Transp Porous Med 79, 117–134. https://doi.org/10.1007/s11242-009-9406-1

Gleeson, T., Manning, A.H., 2008. Regional groundwater flow in mountainous terrain: Three-dimensional simulations of topographic and hydrogeologic controls. Water Resour. Res. 44. https://doi.org/10.1029/2008WR006848

González, F.A., Maksymowicz, A., Díaz, D., Villegas, L., Leiva, M., Blanco, B., Vera, E., Contreras, S., Cabrera, D., Bonvalot, S., 2018. Characterization of the depocenters and the basement structure, below the central Chile Andean Forearc: A 3D geophysical modelling in Santiago Basin area. Basin Res 30, 799–815. https://doi.org/10.1111/bre.12281

Gorelick, N., Hancher, M., Dixon, M., Ilyushchenko, S., Thau, D., Moore, R., 2017. Google Earth Engine: Planetary-scale geospatial analysis for everyone. Remote Sensing of Environment 202, 18–27. https://doi.org/10.1016/j.rse.2017.06.031

Grêt-Regamey, A., Brunner, S.H., Kienast, F., 2012. Mountain Ecosystem Services: Who Cares? Mountain Research and Development 32, S23–S34. https://doi.org/10.1659/MRD-JOURNAL-D-10-00115.S1

Gu, Y., Brown, J.F., Verdin, J.P., Wardlow, B., 2007. A five-year analysis of MODIS NDVI and NDWI for grassland drought assessment over the central Great Plains of the United States. Geophys. Res. Lett. 34, L06407. https://doi.org/10.1029/2006GL029127

Gu, Y., Hunt, E., Wardlow, B., Basara, J.B., Brown, J.F., Verdin, J.P., 2008. Evaluation of MODIS NDVI and NDWI for vegetation drought monitoring using Oklahoma Mesonet soil moisture data. Geophys. Res. Lett. 35, L22401. https://doi.org/10.1029/2008GL035772

Hayashi, M., 2020. Alpine Hydrogeology: The Critical Role of Groundwater in Sourcing the Headwaters of the World. Groundwater 58, 498–510. https://doi.org/10.1111/gwat.12965

Hilberg, S., 2016. Review: Natural tracers in fractured hard-rock aquifers in the Austrian part of the Eastern Alps—previous approaches and future perspectives for hydrogeology in mountain regions. Hydrogeol J 24, 1091–1105. https://doi.org/10.1007/s10040-016-1395-x

Hobouchian, M.P., Salio, P., García Skabar, Y., Vila, D., Garreaud, R., 2017. Assessment of satellite precipitation estimates over the slopes of the subtropical Andes. Atmospheric Research 190, 43–54. https://doi.org/10.1016/j.atmosres.2017.02.006

Hood, J.L., Hayashi, M., 2015. Characterization of snowmelt flux and groundwater storage in an alpine headwater basin. Journal of Hydrology 521, 482–497. https://doi.org/10.1016/j.jhydrol.2014.12.041

Huss, M., Bookhagen, B., Huggel, C., Jacobsen, D., Bradley, R.S., Clague, J.J., Vuille, M., Buytaert, W., Cayan, D.R., Greenwood, G., Mark, B.G., Milner, A.M., Weingartner, R., Winder, M., 2017. Toward mountains without permanent snow and ice. Earth Future 5, 418–435. https://doi.org/10.1002/2016EF000514

Hussien, H.M., Kehew, A.E., Aggour, T., Korany, E., Abotalib, A.Z., Hassanein, A., Morsy, S., 2017. An integrated approach for identification of potential aquifer zones in structurally controlled terrain: Wadi Qena basin, Egypt. Catena 149, 73–85. https://doi.org/10.1016/j.catena.2016.08.032

Immerzeel, W.W., Lutz, A.F., Andrade, M., Bahl, A., Biemans, H., Bolch, T., Hyde, S., Brumby, S., Davies, B.J., Elmore, A.C., Emmer, A., Feng, M., Fernández, A., Haritashya, U., Kargel, J.S., Koppes, M., Kraaijenbrink, P.D.A., Kulkarni, A.V., Mayewski, P.A., Nepal, S., Pacheco, P., Painter, T.H., Pellicciotti, F., Rajaram, H., Rupper, S., Sinisalo, A., Shrestha, A.B., Viviroli, D., Wada, Y., Xiao, C., Yao, T., Baillie, J.E.M., 2020. Importance and vulnerability of the world's water towers. Nature 577, 364–369. https://doi.org/10.1038/s41586-019-1822-y

Jasechko, S., Kirchner, J.W., Welker, J.M., McDonnell, J.J., 2016. Substantial proportion of global streamflow less than three months old. Nature Geosci 9, 126–129. https://doi.org/10.1038/ngeo2636

Jung, Y.-Y., Koh, D.-C., Shin, W.-J., Kwon, H.-I., Oh, Y.-H., Lee, K.-S., 2021. Assessing seasonal variations in water sources of streamflow in a temperate mesoscale catchment with granitic bedrocks using hydrochemistry and stable isotopes. Journal of Hydrology: Regional Studies 38, 100940. https://doi.org/10.1016/j.ejrh.2021.100940

Kamenik, C., Schmidt, R., Kum, G., Psenner, R., 2001. The influence of catchment characteristics on the water chemistry of mountain lakes. Arct. Antarct. Alp. Res. 33, 404–409. https://doi.org/10.2307/1552549

Kaminsky, A., 2010. ZondRes2D. Software for two-dimensional interpretation of DC resistivity and IP data. Zond Geophysical Software, Saint-Petersburg (Russia).

Katsoulas, N., Elvanidi, A., Ferentinos, K.P., Kacira, M., Bartzanas, T., Kittas, C., 2016. Crop reflectance monitoring as a tool for water stress detection in greenhouses: A review. Biosystems Engineering 151, 374–398. https://doi.org/10.1016/j.biosystemseng.2016.10.003

Kolbe, T., Marçais, J., Thomas, Z., Abbott, B.W., de Dreuzy, J.-R., Rousseau-Gueutin, P., Aquilina, L., Labasque, T., Pinay, G., 2016. Coupling 3D groundwater modeling with CFC-based age dating to classify local groundwater circulation in an unconfined crystalline aquifer. Journal of Hydrology 543, 31–46. https://doi.org/10.1016/j.jhydrol.2016.05.020

Kreamer, D.K., Ball, D.M., Re, V., Simmons, C.T., Bothwell, T., Verweij, H.J.M., Mukherjee, A., Moreau, M.F., 2021. Chapter 37 - The future of groundwater science and research, in: Mukherjee, A., Scanlon, B.R., Aureli, A., Langan, S., Guo, H., McKenzie, A.A. (Eds.), Global Groundwater. Elsevier, pp. 503–517. https://doi.org/10.1016/B978-0-12-818172-0.00037-2

Leray, S., de Dreuzy, J.-R., Bour, O., Bresciani, E., 2013. Numerical modeling of the productivity of vertical to shallowly dipping fractured zones in crystalline rocks. Journal of Hydrology 481, 64–75. https://doi.org/10.1016/j.jhydrol.2012.12.014

Leray, S., de Dreuzy, J.-R., Bour, O., Labasque, T., Aquilina, L., 2012. Contribution of age data to the characterization of complex aquifers. Journal of Hydrology 464–465, 54–68. https://doi.org/10.1016/j.jhydrol.2012.06.052

Loke, M.H., 2004. Tutorial: 2-D and 3-D electrical imaging surveys.

Longuevergne, L., Scanlon, B.R., Wilson, C.R., 2010. GRACE Hydrological estimates for small basins: Evaluating processing approaches on the High Plains Aquifer, USA. Water Resour. Res. 46. https://doi.org/10.1029/2009WR008564

Lopez Loera, H., Ramos Leal, J.A., Davila Harris, P., Torres Gaytan, D.E., Martinez Ruiz, V.J., Gogichaishvili, A., 2015. Geophysical Exploration of Fractured-Media Aquifers at the Mexican Mesa Central: Satellite City, San Luis Potosi, Mexico. Surv. Geophys. 36, 167–184. https://doi.org/10.1007/s10712-014-9302-2

Ma, B., Jin, M., Liang, X., Li, J., 2018. Groundwater mixing and mineralization processes in a mountain–oasis–desert basin, northwest China: hydrogeochemistry and environmental tracer indicators. Hydrogeol J 26, 233–250. https://doi.org/10.1007/s10040-017-1659-0

Manning, A.H., Ball, L.B., Wanty, R.B., Williams, K.H., 2021. Direct Observation of the Depth of Active Groundwater Circulation in an Alpine Watershed. Water Res. 57, 2020WR028548. https://doi.org/10.1029/2020WR028548

Manning, A.H., Solomon, D.K., 2005. An integrated environmental tracer approach to characterizing groundwater circulation in a mountain block. Water Resour. Res. 41. https://doi.org/10.1029/2005WR004178

Markovich, K.H., Condon, L.E., Carroll, K.C., Purtschert, R., McIntosh, J.C., 2021. A Mountain-Front Recharge Component Characterization Approach Combining Groundwater Age Distributions, Noble Gas Thermometry, and Fluid and Energy Transport Modeling. Water Res 57. https://doi.org/10.1029/2020WR027743

Markovich, K.H., Manning, A.H., Condon, L.E., McIntosh, J., 2019. Mountain-Block Recharge: A Review of Current Understanding. Water Resour. Res. 55, 8278–8304. https://doi.org/10.1029/2019WR025676

Martos-Rosillo, S., Ruiz-Constán, A., González-Ramón, A., Mediavilla, R., Martín-Civantos, J.M., Martínez-Moreno, F.J., Jódar, J., Marín-Lechado, C., Medialdea, A., Galindo-Zaldívar, J., Pedrera, A., Durán, J.J., 2019. The oldest managed aquifer recharge system in Europe: New insights from the Espino recharge channel (Sierra Nevada, southern Spain). Journal of Hydrology 578, 124047. https://doi.org/10.1016/j.jhydrol.2019.124047

McClymont, A.F., Hayashi, M., Bentley, L.R., Muir, D., Ernst, E., 2010. Groundwater flow and storage within an alpine meadow-talus complex. Hydrol. Earth Syst. Sci. 14, 859–872. https://doi.org/10.5194/hess-14-859-2010

McCord, J.T., Gotway, C.A., Conrad, S.H., 1997. Impact of geologic heterogeneity on recharge estimation using environmental tracers: Numerical modeling investigation. Water Resour. Res. 33, 1229–1240. https://doi.org/10.1029/96WR03755

McDonnell, J.J., 2003. Where does water go when it rains? Moving beyond the variable source area concept of rainfall-runoff response. Hydrol. Process. 17, 1869–1875. https://doi.org/10.1002/hyp.5132

Meyer, J.L., Strayer, D.L., Wallace, J.B., Eggert, S.L., Helfman, G.S., Leonard, N.E., 2007. The contribution of headwater streams to biodiversity in river networks. J. Am. Water Resour. Assoc. 43, 86–103. https://doi.org/10.1111/j.1752-1688.2007.00008.x

Muñoz, M., Hamza, V., 1993. Heat flow and temperature gradients in Chile. Stud Geophys Geod 37, 315–348. https://doi.org/10.1007/BF01624604

Murty, B.V.S., Raghavan, V.K., 2002. The gravity method in groundwater exploration in crystalline rocks: a study in the peninsular granitic region of Hyderabad, India. Hydrogeol. J. 10, 307–321. https://doi.org/10.1007/s10040-001-0184-2

Nicolas, M., Bour, O., Selles, A., Dewandel, B., Bailly-Comte, V., Chandra, S., Ahmed, S., Maréchal, J.-C., 2019. Managed Aquifer Recharge in fractured crystalline rock aquifers: Impact of horizontal preferential flow on recharge dynamics. Journal of Hydrology 573, 717–732. https://doi.org/10.1016/j.jhydrol.2019.04.003

Niemeyer, H., 2002. Historia natural de la Reserva Nacional Río Clarillo: un espacio para aprender ecología. s.n., Santiago.

Pan, S., Wang, Z., Su, Q., Sun, T., Zhang, Y., 2008. Groundwater level monitoring model using multi-temporal images in arid region of northwest China. The International Archives of the Photogrammetry, Remote Sensing and Spatial Information Sciences 37, 745–750.

Piquer, J., Hollings, P., Rivera, O., Cooke, D.R., Baker, M., Testa, F., 2017. Along-strike segmentation of the Abanico Basin, central Chile: New chronological, geochemical and structural constraints. Lithos 268–271, 174–197. https://doi.org/10.1016/j.lithos.2016.10.025

Piquer, J., Rivera, O., Yáñez, G., Oyarzun, N., 2021. The Piuquencillo fault system: a long-lived, Andean-transverse fault system and its relationship with magmatic and hydrothermal activity. Solid Earth 12, 253–273. https://doi.org/10.5194/se-12-253-2021

Rauld, R.A., 2002. Análisis morfoestructural del frente cordillerano Santiago Oriente entre el río Mapocho y la Quebrada de Macul. Tesis geólogo--Universidad de Chile., Santiago de Chile.

Reeves, C., 2005. Aeromagnetic Surveys: Principles, Practice and Interpretation. Geosoft.

Robert, T., Dassargues, A., Brouyere, S., Kaufmann, O., Hallet, V., Nguyen, F., 2011. Assessing the contribution of electrical resistivity tomography (ERT) and self-potential (SP) methods for a water well drilling program in fractured/karstified limestones. J. Appl. Geophys. 75, 42–53. https://doi.org/10.1016/j.jappgeo.2011.06.008

Robinson, D.A., Binley, A., Crook, N., Day-Lewis, F.D., Ferré, T.P.A., Grauch, V.J.S., Knight, R., Knoll, M., Lakshmi, V., Miller, R., Nyquist, J., Pellerin, L., Singha, K., Slater, L., 2008. Advancing process-based watershed hydrological research using near-surface geophysics: a vision for, and review of, electrical and magnetic geophysical methods. Hydrol. Process. 22, 3604–3635. https://doi.org/10.1002/hyp.6963

Roques, C., Bour, O., Aquilina, L., Dewandel, B., Leray, S., Schroetter, Jm., Longuevergne, L., Le Borgne, T., Hochreutener, R., Labasque, T., Lavenant, N., Vergnaud-Ayraud, V., Mougin, B., 2014. Hydrological behavior of a deep sub-vertical fault in crystalline basement and relationships with surrounding reservoirs. Journal of Hydrology 509, 42–54. https://doi.org/10.1016/j.jhydrol.2013.11.023

Ruelleu, S., Moreau, F., Bour, O., Gapais, D., Martelet, G., 2010. Impact of gently dipping discontinuities on basement aquifer recharge: An example from Ploemeur (Brittany, France). J. Appl. Geophys. 70, 161–168. https://doi.org/10.1016/j.jappgeo.2009.12.007

Ruiz-Pereira, S., Díez, B., Cifuentes-Anticevic, J., Leray, S., Fernandoy, F., Marquardt, C., Lambert, F., 2023. Hydrological connections in a glaciated Andean catchment under permafrost conditions (33°S). Journal of Hydrology: Regional Studies 45, 101311. https://doi.org/10.1016/j.ejrh.2022.101311

Samouelian, A., Cousin, I., Tabbagh, A., Bruand, A., Richard, G., 2005. Electrical resistivity survey in soil science: a review. Soil Tillage Res. 83, 173–193. https://doi.org/10.1016/j.still.2004.10.004

Sanford, W., 2002. Recharge and groundwater models: an overview. Hydrogeology Journal 10, 110–120. https://doi.org/10.1007/s10040-001-0173-5

Sanhueza, J., Yáñez, G., Barra, F., Maringue, J., Figueroa, R., Saez, E., 2022. Rheological, petrophysical and geometrical constraints of a subduction channel from a numerical model perspective: Insights from La Cabana Paleozoic peridotites, Coastal Cordillera of south-central Chile. J. South Am. Earth Sci. 114, 103706. https://doi.org/10.1016/j.jsames.2021.103706

Schaaf, C., Wang, Z., 2015. MCD43A4 MODIS/Terra+Aqua BRDF/Albedo Nadir BRDF Adjusted Ref Daily L3 Global - 500m V006. https://doi.org/10.5067/MODIS/MCD43A4.006

Schaller, M.F., Fan, Y., 2009. River basins as groundwater exporters and importers: Implications for water cycle and climate modeling. J. Geophys. Res. 114, D04103. https://doi.org/10.1029/2008JD010636

Scibek, J., Gleeson, T., McKenzie, J.M., 2016. The biases and trends in fault zone hydrogeology conceptual models: global compilation and categorical data analysis. Geofluids 16, 782–798. https://doi.org/10.1111/gfl.12188

Seeyan, S., Merkel, B., Abo, R., 2014. Investigation of the Relationship between Groundwater Level Fluctuation and Vegetation Cover by using NDVI for Shaqlawa Basin, Kurdistan Region – Iraq. JGG 6, p187. https://doi.org/10.5539/jgg.v6n3p187

Seibert, J., McDonnell, J.J., 2015. Gauging the Ungauged Basin: Relative Value of Soft and Hard Data. J. Hydrol. Eng. 20, A4014004. https://doi.org/10.1061/(ASCE)HE.1943-5584.0000861

Somers, L.D., Gordon, R.P., McKenzie, J.M., Lautz, L.K., Wigmore, O., Glose, A., Glas, R., Aubry-Wake, C., Mark, B., Baraer, M., Condom, T., 2016. Quantifying groundwater–surface water interactions in a proglacial valley, Cordillera Blanca, Peru. Hydrol. Process. 30, 2915–2929. https://doi.org/10.1002/hyp.10912

Somers, L.D., McKenzie, J.M., 2020. A review of groundwater in high mountain environments. WIREs Water 7. https://doi.org/10.1002/wat2.1475

Soulsby, C., Tetzlaff, D., van den Bedem, N., Malcolm, I.A., Bacon, P.J., Youngson, A.F., 2007. Inferring groundwater influences on surface water in montane catchments from hydrochemical surveys of springs and streamwaters. J. Hydrol. 333, 199–213. https://doi.org/10.1016/j.jhydrol.2006.08.016

Telford, W.M., Geldart, L.P., Sheriff, R.E., 1990. Applied Geophysics, 2nd ed. Cambridge University Press. https://doi.org/10.1017/CBO9781139167932

Thiele, R., 1980. Hoja Santiago: región metropolitana: carta geológica de Chile escala 1: 250.000. Instituto de Investigaciones Geológicas, Chile.

Troldborg, L., Refsgaard, J.C., Jensen, K.H., Engesgaard, P., 2007. The importance of alternative conceptual models for simulation of concentrations in a multi-aquifer system. Hydrogeol J 15, 843–860. https://doi.org/10.1007/s10040-007-0192-y

Valdenegro, P., Muñoz, M., Yáñez, G., Parada, M.A., Morata, D., 2019. A model for thermal gradient and heat flow in central Chile: The role of thermal properties. Journal of South American Earth Sciences 91, 88–101. https://doi.org/10.1016/j.jsames.2019.01.011

Vittecoq, B., Reninger, P.-A., Lacquement, F., Martelet, G., Violette, S., 2019. Hydrogeological conceptual model of andesitic watersheds revealed by high-resolution heliborne geophysics. Hydrol. Earth Syst. Sci. 23, 2321–2338. https://doi.org/10.5194/hess-23-2321-2019

Viviroli, D., Archer, D.R., Buytaert, W., Fowler, H.J., Greenwood, G.B., Hamlet, A.F., Huang, Y., Koboltschnig, G., Litaor, M.I., Lopez-Moreno, J.I., Lorentz, S., Schaedler, B., Schreier, H., Schwaiger, K., Vuille, M., Woods, R., 2011. Climate change and mountain water resources: overview and recommendations for research, management and policy. Hydrol. Earth Syst. Sci. 15, 471–504. https://doi.org/10.5194/hess-15-471-2011

Viviroli, D., Kummu, M., Meybeck, M., Kallio, M., Wada, Y., 2020. Increasing dependence of lowland populations on mountain water resources. Nat. Sustain. 3, 917-+. https://doi.org/10.1038/s41893-020-0559-9

Welch, L.A., Allen, D.M., 2012. Consistency of groundwater flow patterns in mountainous topography: Implications for valley bottom water replenishment and for defining groundwater flow boundaries. Water Resour. Res. 48. https://doi.org/10.1029/2011WR010901

Weyer, C., Peiffer, S., Schulze, K., Borken, W., Lischeid, G., 2014. Catchments as heterogeneous and multi-species reactors: An integral approach for identifying biogeochemical hot-spots at the catchment scale. Journal of Hydrology 519, 1560–1571. https://doi.org/10.1016/j.jhydrol.2014.09.005

White, B.A., Burbey, T.J., 2007. Evidence for structurally controlled recharge in the Blue Ridge Province, Virginia, USA. Hydrogeol J 15, 929–943. https://doi.org/10.1007/s10040-006-0150-0

Wilson, J.L., Guan, H., 2004. Mountain-block hydrology and mountain-front recharge, in: Hogan, J.F., Phillips, F.M., Scanlon, B.R. (Eds.), Water Science and Application. American Geophysical Union, Washington, D. C., pp. 113–137. https://doi.org/10.1029/009WSA08

Winter, T.C., 2001. The concept of hydrological landscapes. J Am Water Resources Assoc 37, 335–349. https://doi.org/10.1111/j.1752-1688.2001.tb00973.x

Yáñez, G., Munoz, M., Flores-Aqueveque, V., Bosch, A., 2015. Gravity derived depth to basement in Santiago Basin, Chile: implications for its geological evolution, hydrogeology, low enthalpy geothermal, soil characterization and geo-hazards. Andean Geol. 42, 147–172. https://doi.org/10.5027/andgeoV42n2-a01

Yáñez, G., Perez-Estay, N., Araya-Vargas, J., Sanhueza, J., Figueroa, R., Maringue, J., Rojas, T., 2020. Shallow Anatomy of the San Ramon Fault (Chile) Constrained by Geophysical Methods: Implications for its Role in the Andean Deformation. Tectonics 39, e2020TC006294. https://doi.org/10.1029/2020TC006294

Zambrano-Bigiarini, M., Nauditt, A., Birkel, C., Verbist, K., Ribbe, L., 2017. Temporal and spatial evaluation of satellite-based rainfall estimates across the complex topographical and climatic gradients of Chile. Hydrol. Earth Syst. Sci. 21, 1295–1320. https://doi.org/10.5194/hess-21-1295-2017

8. Tables and Illustrations

	Measured density (g/cc)	Measured magnetic susceptibility (SI)
Intrusive rocks	2.64 +- 0.03	0.04 +- 0.01
Volcanic rocks	2.73 +- 0.09	0.27 +- 0.18

Table 1: Mean measured density (g/cc) and mean magnetic susceptibility (SI) for rock samples collected on the field (20 samples)

Model	Main process	Surface drained (km^2)	Main geological structures involved
1	Local drainage from lateral hillslope	3-9	Alluvial deposits
2	Upstream groundwater exfiltration deriving from groundwater seepage area reduction	97	Pluton-volcanic rocks contact
3	Water export from Los Bueyes catchment	12	Papagayo N-S regional fault, including secondary E-W local fault system

949 Table 2: Summary of possible conceptual models associated with their main process and the geological
950 structure involved. Contribution surface values corresponds to Figure 7 area.

951

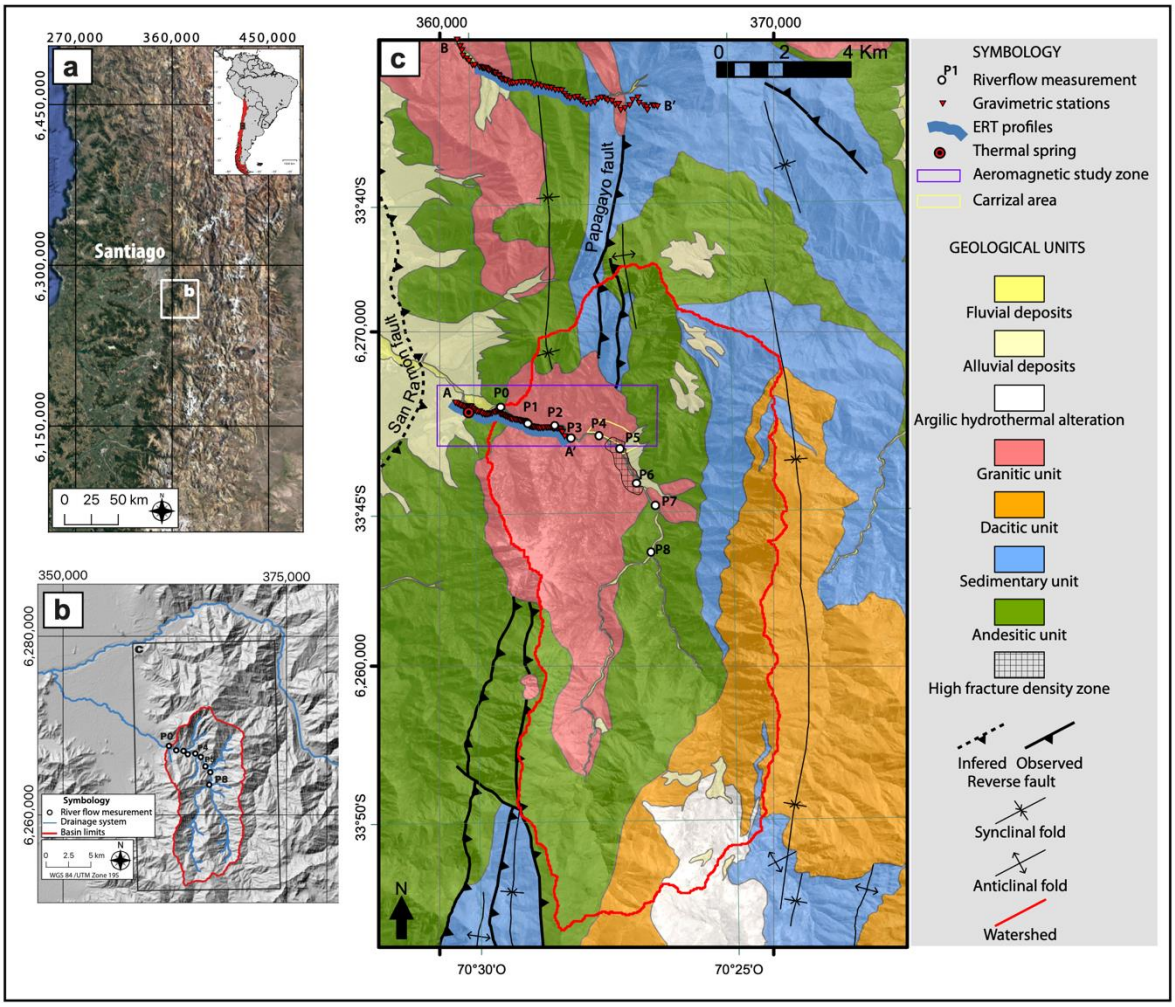

Figure 1: a) Satellite view of the Santiago area, the white rectangle outlines the study area. b) Topographic map overlaid with the Parque Nacional del Río Clarillo catchment limits, the drainage system and the streamflow measurement points (numbered in increasing order from P0 to P8 going upstream) c) geological map of the study area overlaid with the ERT profile (blue lines), the gravimetric profile (red triangles), the area covered by the aeromagnetic flights (areas delimited by purple line) and the river flow measurements (white dots surrounded by black). A 23°C perennial thermal spring located at the exit of the Parque Nacional del Río Clarillo is indicated with a red dot.

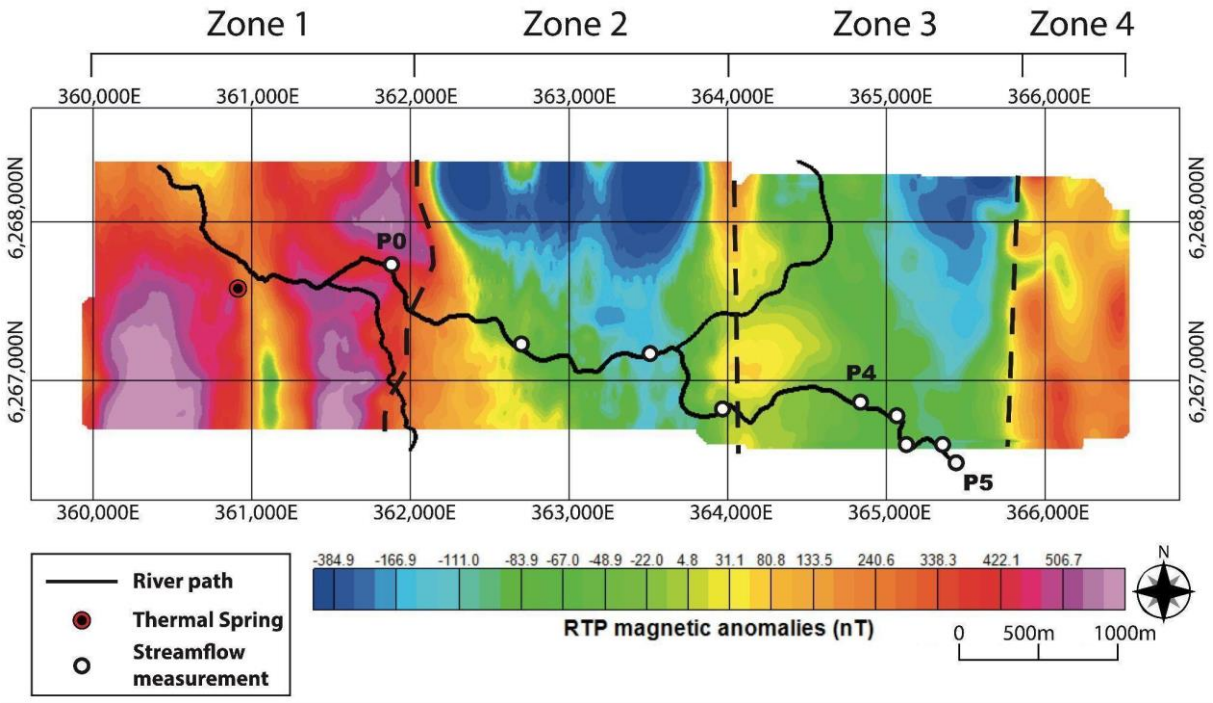

Figure 2: Aeromagnetic anomaly map (reduced to the pole) for the Río Clarillo area (Figure 1, purple rectangle). Dashed lines represent the limit between magnetic zones.

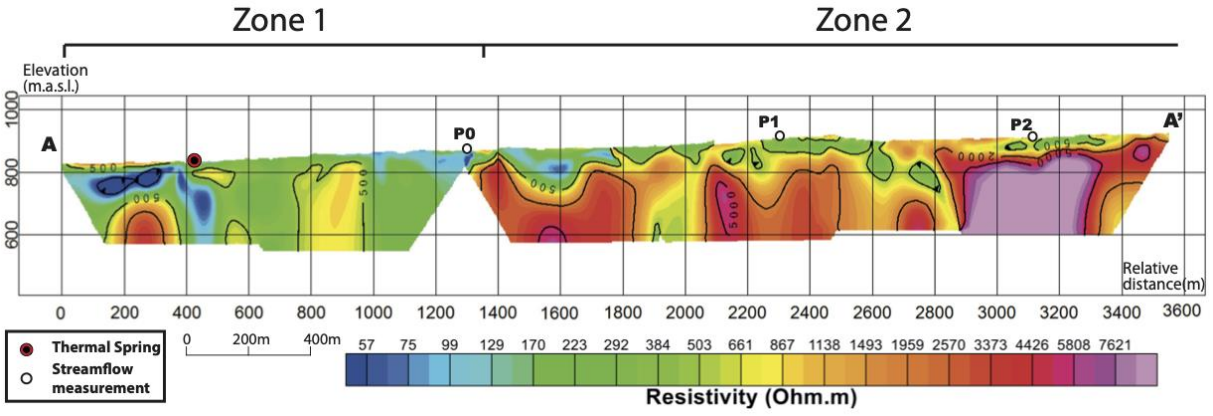

Figure 3: Electrical resistivity model for the Río Clarillo transect (A-A', Figure 1). Projections of the hydraulic markers on the profile (red dot for the thermal spring and white dots for the river flow measurements) as well as the magnetic zones limits (Figure 2) presented over the transect.

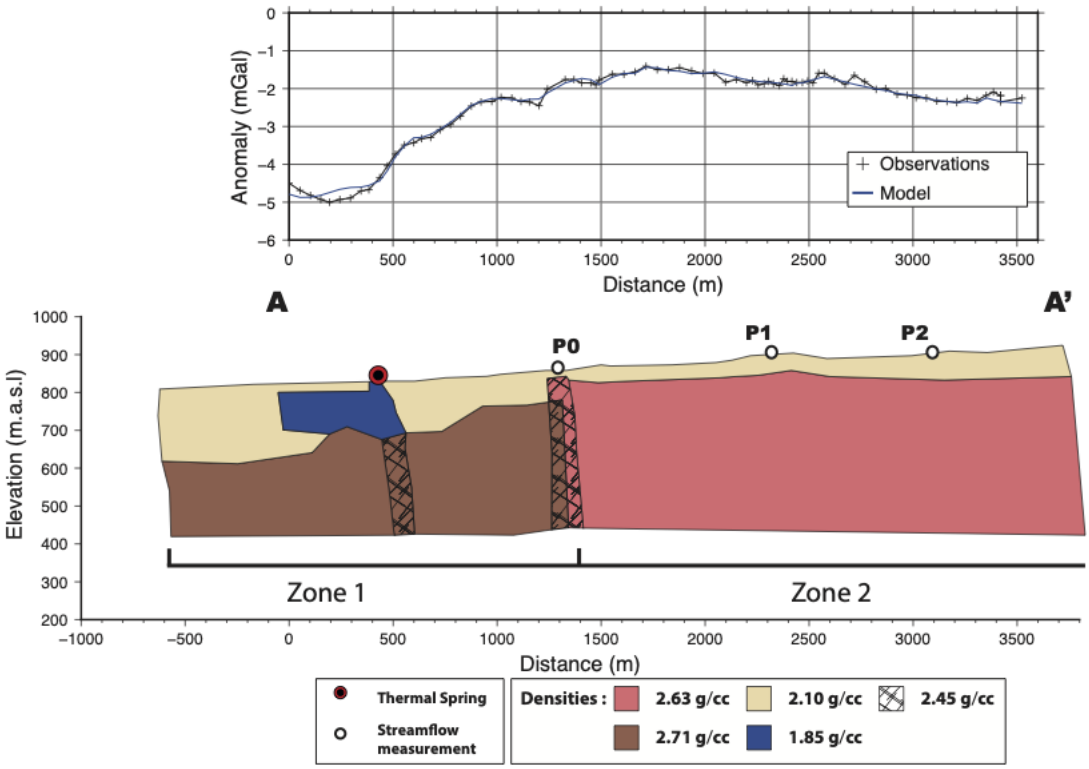

969

970 Figure 4: Representation of the gravity study for the Río Clarillo transect (A-A', Figure 1) and the
971 associated interpretation derived from geophysical and geological constraints. Top: The black line with
972 crosses represents the data (each cross is one data point), the blue line represents the fit of the model
973 described above. Bottom: Model representing the gravity data based on density variations. For a better
974 understanding, it includes projections of the hydraulic markers on the profile (red dot for the thermal
975 spring and white dots for the river flow measurements) as well as the magnetic zones limits (Figure 2)
976 presented above the transect.

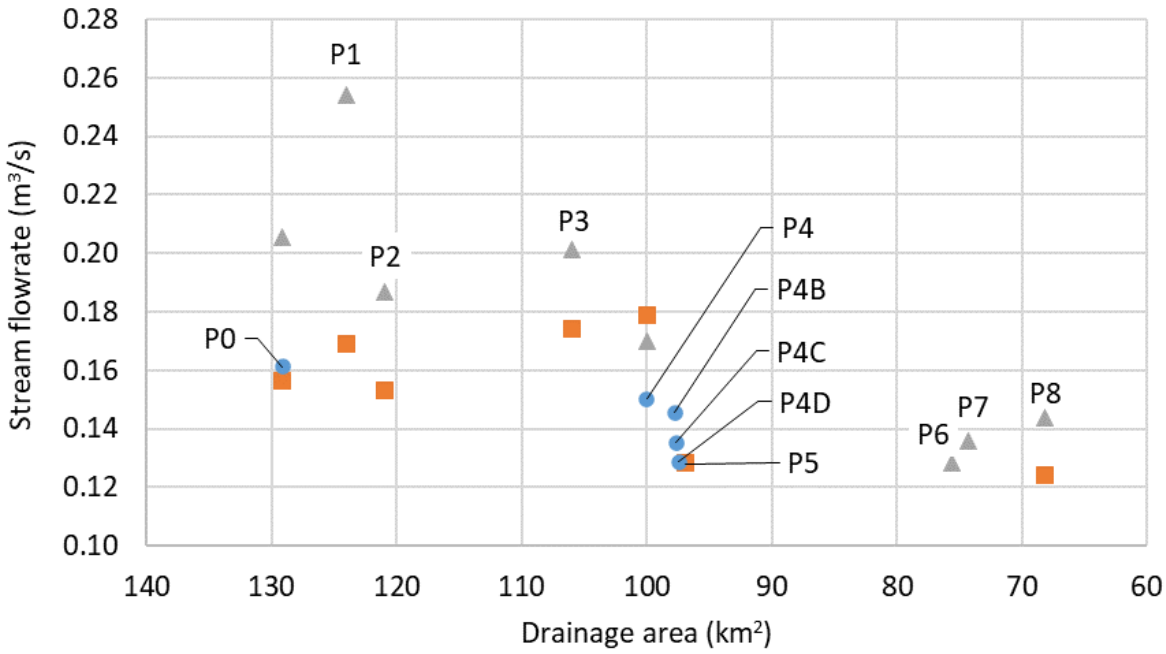

977

978 Figure 5: Streamflow rate during the 2019 recession period (austral autumn) as a function of drainage
979 area. P0 point corresponds to the outlet of the Parque Nacional del Río Clarillo catchment (*i.e.*,
980 downstream at the Andes piedmont) while P8 corresponds to the confluence of the two main
981 affluents, approximately 9 km upstream. Orange square corresponds to March 2019 campaign, blue
982 circle corresponds to April 2019 resampling campaign and grey triangle corresponds to the June 2019
983 campaign.

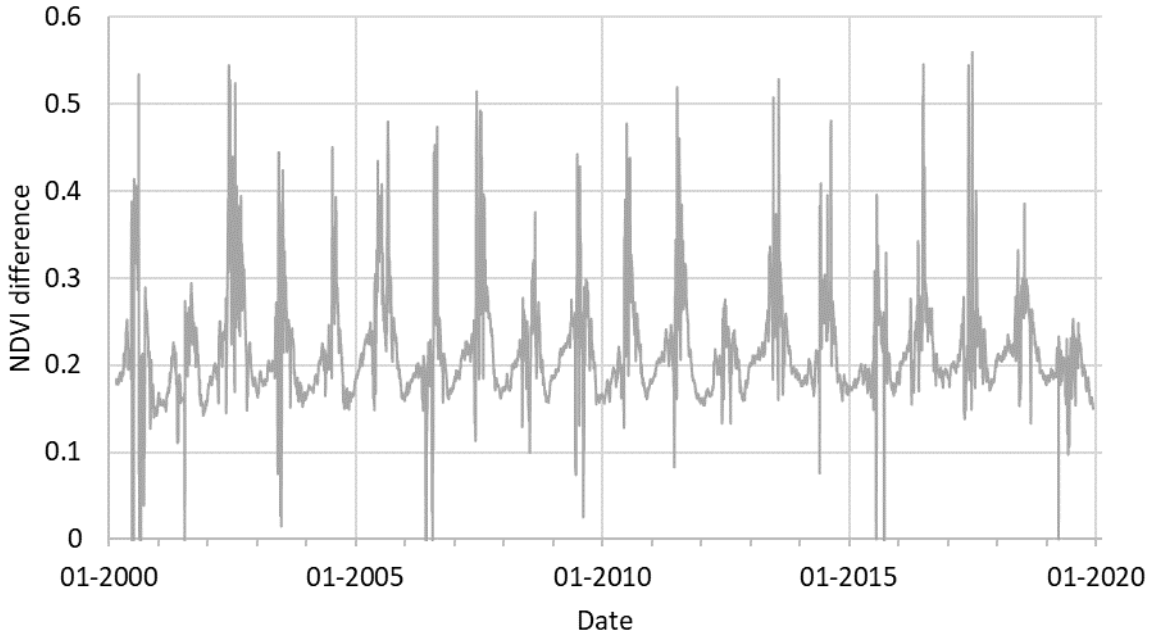

984

985 Figure 6: Difference between the mean NDVI of the Carrizal area and the mean NDVI of the entire

986 National Park for the period 2000-2019, included.

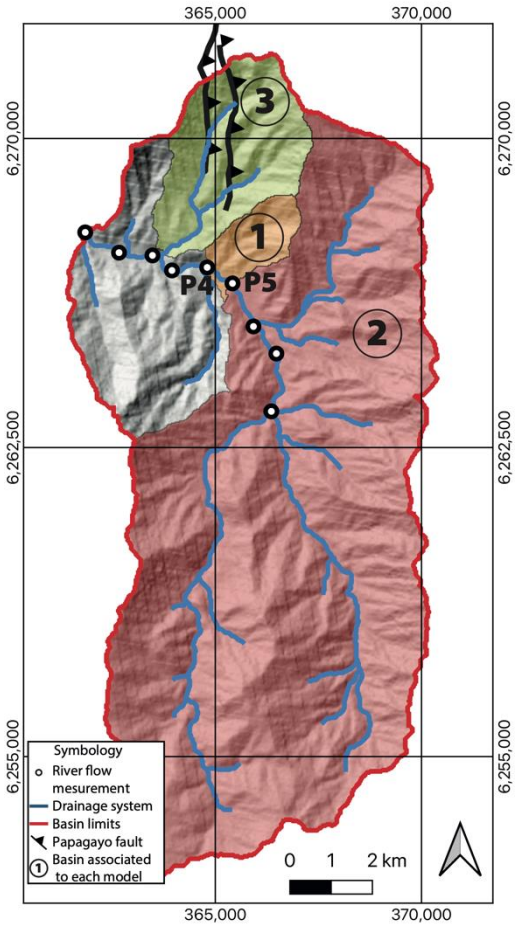

Figure 7: Representation of the Parque Nacional Río Clarillo catchment with river network (blue lines) and river flow measurements (black-circled white dots). Numbers 1 to 3 correspond to the possible drainage areas contributing to the resurgence between points P4 and P5, based on the three models mentioned in sections 2.5 and 4.1. Grey area within the catchment is not part of any of the proposed models.